

# Wind tunnel test on mean wind forces and peak pressure acting on ellipsoidal nacelles of wind turbine

Wind Engineering

1–16

© The Author(s) 2021

Article reuse guidelines:

[sagepub.com/journals-permissions](https://sagepub.com/journals-permissions)

DOI: 10.1177/0309524X211044511

[journals.sagepub.com/home/wie](https://journals.sagepub.com/home/wie)**Hiroshi Noda<sup>1</sup>**  and **Takeshi Ishihara<sup>2</sup>**

## Abstract

Mean wind forces and peak pressures acting on ellipsoidal nacelles are investigated by wind tunnel tests. The wind force coefficients of the ellipsoidal nacelles for the wind turbine design and the peak pressure coefficients for the nacelle cover design are proposed based on the experimental data. The wind force coefficients are expressed as functions of yaw angles. The proposed formulas are compared with Eurocode, Germanischer Lloyd and ASCE7-16. It is found that the mean wind force coefficients for the wind turbine nacelles are slightly underestimated in Eurocode. The equivalent maximum and minimum mean pressure coefficients are proposed for use in Design Load Case 6.1 and Design Load Case 6.2 of IEC 61400-1. The peak pressure coefficients are derived using a quasi-steady theory. The proposed equivalent maximum and minimum mean pressure coefficients are much larger than those specified in Germanischer Lloyd.

## Keywords

Wind turbine, ellipsoidal nacelle, wind tunnel test, mean wind force coefficient, peak pressure coefficient, wind resistant design

## Introduction

Investigations and considerations of the safety against strong winds are required since a good place to build a wind turbine is generally a windy site. Therefore, the wind turbine is exposed to strong winds in the extreme wind conditions. In these sites, strong winds, such as typhoon, hurricane, and cyclone, might pass frequently and wind resistant design for wind turbines is an important issue.

Numerous researches have been conducted on the wind forces acting on blades (Chou et al., 2013; Esfahanian et al., 2013; Hu et al., 2012; Lee et al., 2012) and towers (Ishihara et al., 2005). The reasons seem to be that the blades are the main components that determine the power production efficiency and the tower is the main structure that supports the wind turbine equipment itself. Many studies concerning basic shapes such as wings (Abbott and Von Doenhoff, 1959; Rafiee et al., 2016; Schmitz, 1942) and cylinders (Rajani et al., 2016; Roshko, 1961; Williamson, 1996) have been conducted using wind tunnel experiments, computational fluid dynamics, and full-scale measurements. On the other hand, it is hard to find the studies concerning wind forces and pressures acting on the nacelles, particularly those for the purpose of the wind resistant design of nacelle, including the small hatch on the surface of the nacelle. It is often simplified in the wind resistant design of the wind turbine structure. However, the nacelle is an important component that houses drive trains, generators, control systems, etc., namely, damage to the nacelle is directly linked to turbine shutdown. Nevertheless, the engineering basis required for wind resistant design, such as the suitable wind force coefficients of nacelle is few existence. The local peak pressure acting on the nacelle cover is rarely considered when designing the wind turbine nacelle. A guide for the design of wind turbines, the ASCE/AWEA RP (2011), describes recommendations for not only the wind resistant design of

<sup>1</sup>Department of Architecture, Kindai University, Higashiosaka, Osaka, Japan

<sup>2</sup>Department of Civil Engineering, The University of Tokyo, Bunkyo-ku, Tokyo, Japan

## Corresponding author:

Hiroshi Noda, Department of Architecture, Kindai University, 3-4-1 Kowakae, Higashiosaka, Osaka 577-8502, Japan.

Email: [hnodea@arch.kindai.ac.jp](mailto:hnodea@arch.kindai.ac.jp)

wind turbines but also for the whole stages from planning to operation and maintenance. In this document, the importance of the wind load of rotor-nacelle assembly is described because the wind loads on it are generally larger than the wind loads on towers. However, there is no recommended value for the wind force coefficient of the rotor-nacelle assembly itself.

Significant accidents due to damage to the nacelle cover have been reported in Japan (METI of Japan, 2016, 2017). Ishihara et al. (2005) has been pointed out that the underestimation of the wind load of the nacelle cover in the design process was responsible for the damages. Since the nacelle is a bluff body, it may be possible to determine the wind force and pressure coefficients of the nacelle by referring to the wind force and surface pressure coefficients of a square cube or sphere. However, the wind resistant design of the nacelle requires wind force coefficients and pressure coefficients under the specific conditions, such as less turbulence due to the high elevation from the ground, the influence of the blades and tower, and limited wind directions by the yaw control. Moreover, the nacelle consists of several covers and hatches, the wind force coefficients for structural design and the peak wind pressure coefficients for component design are required as those in the wind resistant design of the buildings (ASCE7-16, 2016; European Committee for Standardization, 2005 (hereinafter referred to as Eurocode (2005))).

Noda and Ishihara (2014) investigated the wind forces and pressures on the rectangular type nacelles for the first time. The equivalent mean wind pressure coefficients which can be translated to the peak value using turbulent intensity were proposed for nacelle cover design. These results have been adopted on “Guidelines for Design of Wind Turbine support Structures and Foundations” (Ishihara, 2010) in Japan. However, Noda and Ishihara (2014) have covered only rectangular type nacelles. Goit and Ishihara (2020) conducted a series of wind tunnel experiments on the rectangular and the ellipsoidal nacelles with the different turbulence intensities in the incident flow. They investigated the effects of the turbulence intensity on the aerodynamic coefficients acting on the nacelles, however, the formulas of the mean wind force coefficients for each yaw angle were not proposed, and the maximum and minimum peak pressure coefficients in all yaw angle were not investigated.

The mean wind force coefficients for structural design and the equivalent mean wind pressure coefficients for nacelle cover design of the elliptical nacelles are investigated in this study. The wind tunnel experiments are conducted to measure the wind force acting on the whole elliptical nacelle and the wind pressure acting on the surface of the nacelle. Section 2 describes the wind tunnel experiment setup and conditions. The measurement of the peak pressure and the estimation of statistical values of them are described in detail. The wind forces acting on the entire nacelle are then discussed. The wind force coefficients for structural design of the ellipsoidal nacelle are proposed and compared with that proposed in Germanischer Lloyd (2010), Eurocode (2005), and ASCE7-16 (2016) in Section 3. The mean and peak wind pressure coefficients are investigated, and the equivalent mean pressure coefficients corresponding to Design Load Case 6.1 and Design Load Case 6.2 (hereinafter referred to as DLC 6.1 and DLC 6.2, respectively) of IEC61400-1 (2019) are proposed in Section 4. Finally, the conclusions of this study are summarized in Section 5.

## Experimental setup

Wind tunnel experimental facilities used in wind force measurement was different from that used in peak wind pressure experiment. In the wind force measurement, we used the same wind tunnel experimental facility as Noda and Ishihara (2014). On the other hand, for the experiment to measure the peak wind pressure, a wind tunnel experiment facility owned by the University of Tokyo was used, the details of which is described later.

### *Experimental facilities and characteristics of incident flow*

The wind tunnel experimental facility and the characteristics of incident flow used in the wind force experiment were described in Noda and Ishihara (2014) in detail. Two types of flow which were smooth flow with a turbulence intensity of 0.2% and turbulent boundary layer flow were used as incident flows. Turbulence intensity of turbulent boundary layer flow was approximately 13% at nacelle height. The wind tunnel experiment facility used in the peak pressure experiment was the Gottingen type boundary layer wind tunnel with a test section size of 1.8 m (height)  $\times$  1.5 m (width)  $\times$  11.0 m (length). Turbulent boundary layer flow were used as incident flows in peak pressure experiments. Profiles of mean wind velocity and turbulence intensity (The value obtained by dividing the standard deviation of wind velocity by the mean wind velocity.) of incident flow in peak pressure experiments are shown in Figure 1. Power law exponent  $\alpha$  was 0.2 which is almost same with that of wind force experiment. Turbulence intensity at nacelle height was approximately 13%.

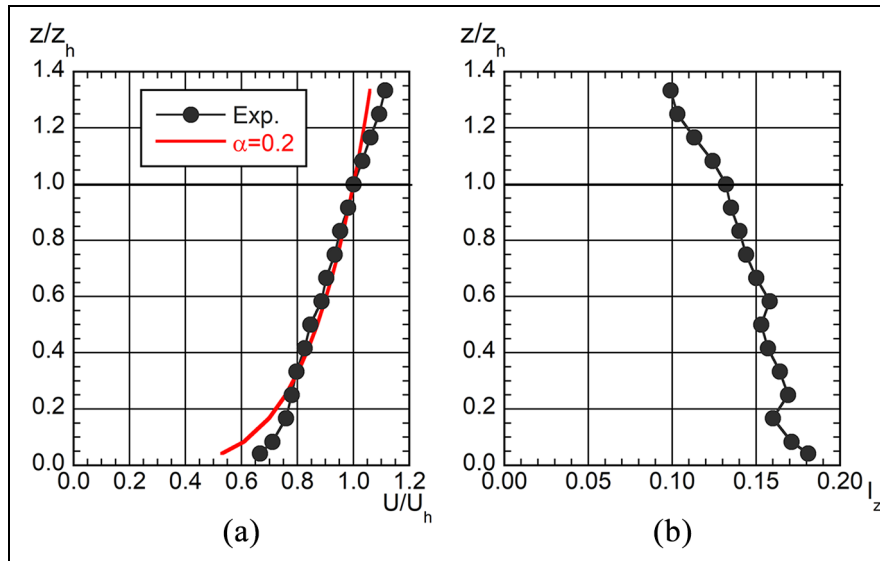


**Figure 1.** Characteristics of the incident flow of mean wind force measurement: (a) vertical profile of mean wind velocity and (b) turbulence intensity,  $z$  is height from wind tunnel floor,  $z_h$  is the nacelle height,  $U$  is mean wind velocity at  $z$ ,  $U_h$  is the mean wind velocity at  $z_h$ ,  $I_z$  is turbulent intensity at  $z$ .

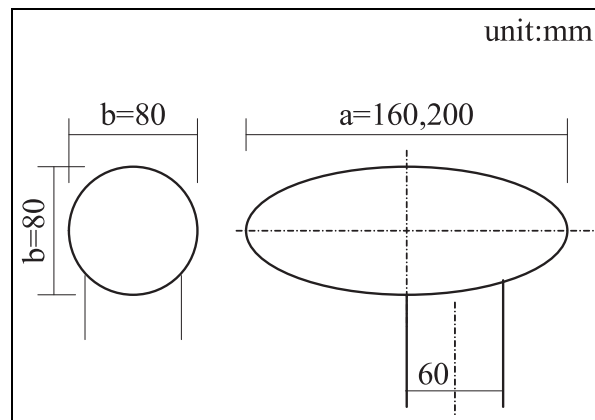


**Figure 2.** Experimental models.

### Mean wind force measurements

The nacelle type chosen in this study is ellipsoidal, because this type is the second most commonly used after the rectangular type investigated in Noda and Ishihara (2014). The nacelle models had aspect ratios ( $a/b$ ) of 2.0 and 2.5 which were determined by a survey of actual nacelle configurations and are shown in Figure 2. The models were scaled to 1/50 and a schematic view of the model setup is shown in Figure 3. The nacelle models were connected to a load cell by a support rod that was shielded by a tower. The capacity range of the load cell was  $\pm 5$  kg. The definitions of the wind forces and yaw angle are shown in Figure 4. The yaw angle is defined so that front surface is normal to the wind direction for  $\theta = 0^\circ$ , with clockwise indicating a positive yaw angles.

Wind force measurements were conducted for the eight cases shown in Table 1, in order to investigate the effects of the Reynolds number, turbulence in the incident flow, and nacelle length. When investigating the influence due to the Reynolds number, it is necessary to vary the experimental wind velocity in the range of 2–3 orders of magnitude. This variation of the experimental wind velocity, however, is practically difficult to achieve. Referring to Buresti (1981), which considers the Reynolds number effects on cylinders by using surface roughness instead of

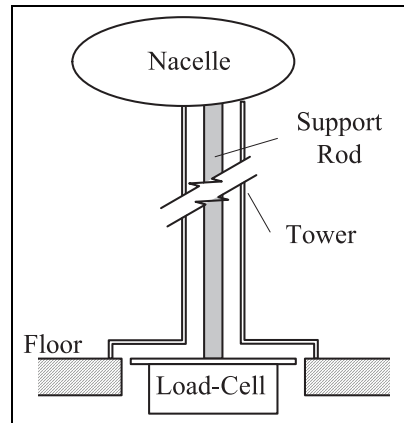


**Figure 3.** Setup of models in wind force measurements.

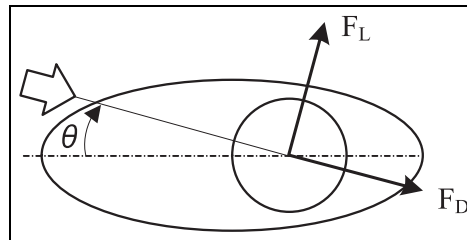


**Figure 4.** Definitions of force and yaw angles.

**Table 1.** Experimental cases for wind force measurement: a and b are shown in Figure 2.

Case no.	Surface roughness	Intensity at nacelle height (%)	Aspect ratio
Case 1	without	0.2	$a/b = 2.0$
Case 2	without	0.2	$a/b = 2.5$
Case 3	with	0.2	$a/b = 2.0$
Case 4	with	0.2	$a/b = 2.5$
Case 5	without	13.2	$a/b = 2.0$
Case 6	without	13.2	$a/b = 2.5$
Case 7	with	13.2	$a/b = 2.0$
Case 8	with	13.2	$a/b = 2.5$

varying wind speed or viscosity, we added surface roughness to the nacelle model to reproduce the effect of Reynolds number. The surface roughness was reproduced by attaching rubber net with a blockage ratio of 23% (diameter of about 1 mm, spacing of about 8 mm). The blockage ratio of rubber net was determined by referring to the results of Ohkuma et al. (1986). Ohkuma et al. (1986) indicated that the mean roughness density at which the turbulent boundary layer is most likely to develop is between 10% and 30%. The height of tower was set to 400 mm for wind force measurement and 600 mm for surface pressure measurement, respectively. These height are lower than the actual height of a wind turbine tower but these are sufficient to avoid the effects of the ground on the wind force acting on the nacelle during the measurement. Examples of the model setup are shown in Figure 5. The experimental conditions for the mean wind force measurements are summarized in Table 2. Sampling time  $\Delta t$  was 10 ms (100 Hz), and the sampling number was 30,000. The yaw angle was varied from  $0^\circ$  to  $180^\circ$  at  $5^\circ$  intervals. The wind velocity for the mean wind force measurement was set to 8 m/s. The Reynolds number based on the nacelle depth (80 mm) and the wind velocity (8.0 m/s) at the nacelle height and was  $4.41 \times 10^4$  in case of the mean wind force measurements.

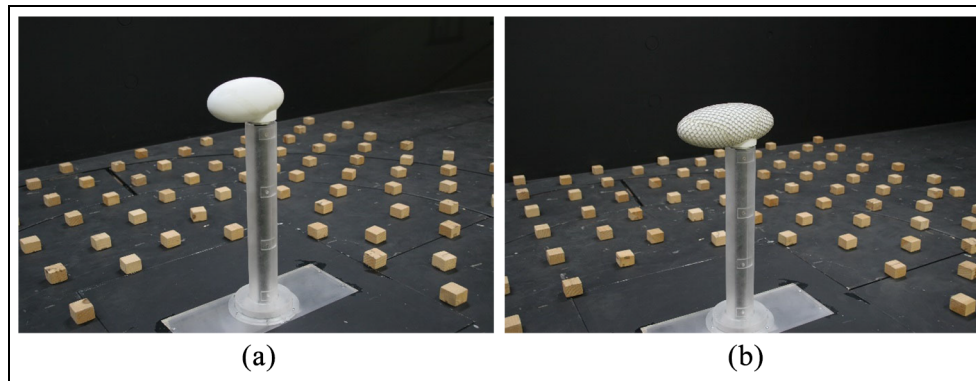


**Figure 5.** Examples of experimental setups for wind force measurements: (a) case5  $a/b = 2.0$  without surface roughness and (b) case8  $a/b = 2.5$  with surface roughness.

**Table 2.** Experimental conditions.

	Mean wind force measurements	Surface pressure measurements
Incident flows	Smooth flow/boundary layer flow	Boundary layer flow
Turbulent intensity (%)	0.2 / 13	13
Length scale	1 / 50	1/50
Wind speed at nacelle height (m/s)	8	5.5
Reynolds number* ( $\times 10^4$ )	4.41	3.03
Sampling time	10 ms (100 Hz)	1.92 ms (512 Hz)
Number of data	30,000	32,768
Number of samples	1	5
Yaw angles	$0^\circ - 180^\circ$	$0^\circ - 355^\circ$

\*Based on nacelle depth (=0.08 m).

### Surface pressure measurements

The experimental model used for the surface pressure measurements was a model with the aspect ratio ( $a/b$ ) of 2.5. The measurement was conducted in the turbulent boundary layer flow, the same as in case 6 for the wind forces measurements. All of the surface pressures were measured using pressure transducers connected to the surface pressure orifices via vinyl tubes. The range of each pressure transducer was  $\pm 1250$  Pa. The sensitivity was 125 Pa/V. The amplifications and time delays of fluctuating pressures due to the effect of the vinyl tubing were corrected by using the method proposed by Irwin et al. (1979). In all, 160 pressure orifices were symmetrically arranged on one half-side of the model as shown in Figure 6. The wind velocity for the surface pressure measurements was 5.5 m/s. In the surface pressure measurements, the Reynolds number based on the nacelle depth (0.08 m) and the wind velocity (5.5 m/s) at the nacelle height was  $3.03 \times 10^4$ . The experimental conditions of the surface pressure measurements are also summarized in Table 2. The number of samples corresponds to the number of data-set (number of measuring) at one yaw angle. In case of evaluating mean wind pressure, one data set whose number is 32,768, might be enough. However, the peak pressures vary widely, and therefore, five maximum values (one maximum value from one data-set) were averaged to obtain maximum peak pressure coefficients.

To make evaluation of the peak values of the wind pressure that acts on a finite area, multiple pressure orifices must be arranged within that finite area and averaged in space. Instead of averaging the pressure in space, a moving average approach has been proposed by Lawson (1980) and was applied to the time series of a sample of pressures using the equivalent averaging time  $T_c$ .  $T_c$  was calculated using reference length, wind velocity, and decay factor which were investigated and proposed by Noda and Ishihara (2014), Lawson (1980). The moving average number  $N$  was determined as 4 following the same manner of previous study (Lawson, 1980; Noda and Ishihara, 2014).

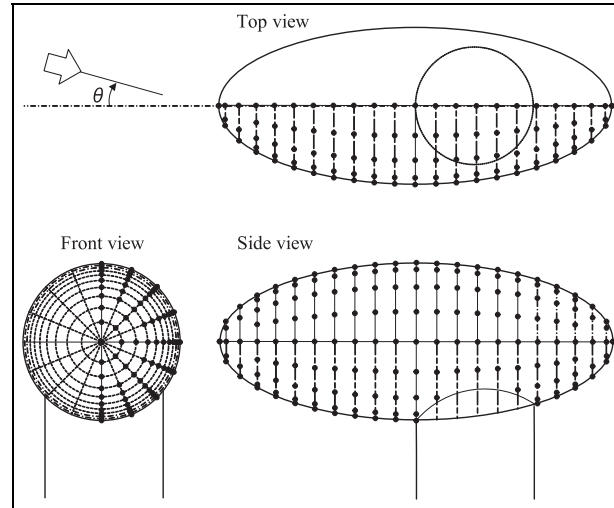


**Figure 6.** Pressure measurement orifices on nacelle model.

### Mean wind force coefficients

This section discusses the characteristics of the mean drag and lift coefficients obtained by the mean wind force measurements. First, the effects of various factors, such as Reynolds number (pseudo investigation using addition of surface roughness), turbulence in the incident flow and nacelle length, on the wind force coefficients are examined. After that, formulas for the mean drag and lift coefficients for wind resistant design are proposed using same procedure in Noda and Ishihara (2014) and compared with the current wind resistant design standard and code.

#### Definitions of wind force coefficients

The mean drag force coefficient ( $C_D(\theta)$ ) and mean lift force coefficient ( $C_L(\theta)$ ) are defined as in equations (1) and (2), respectively:

$$C_D(\theta) = \frac{F_D(\theta)}{\frac{1}{2}\rho U_h^2 A} \quad (1)$$

$$C_L(\theta) = \frac{F_L(\theta)}{\frac{1}{2}\rho U_h^2 A} \quad (2)$$

where,  $F_D(\theta)$  is the mean (i.e. time averaged) drag force,  $F_L(\theta)$  is the mean lift force,  $\rho$  is the air density,  $\theta$  is the yaw angle,  $U_h$  is the wind velocity at the nacelle height, and  $A$  is a reference area as defined in equation (3)

$$A = \frac{\pi ab}{4} \quad (3)$$

where,  $a$  and  $b$  are the length and width of nacelle respectively (refer to Figure 2), and  $\pi$  is the circular constant (pi).

#### Effects of various factors on mean wind force coefficients

The various effects on mean wind force coefficients are discussed in this section. In the beginning, mean drag coefficients and mean lift coefficients of  $a/b = 2.5$  in smooth flow (in Case 2 and Case 4) are shown in Figure 7(a) and (b), as examples of the effects of surfaces roughness. Slightly increase in  $C_D$  in the range from  $\theta = 0^\circ$  to  $60^\circ$ , around  $180^\circ$  and decrease in  $C_L$  around  $\theta = 30^\circ$  and  $130^\circ$  can be seen in case of with surface roughness compared to without surface roughness. This tendency was almost same in case of turbulent boundary layer flow and in case of other aspect ratio of 2.0. The result that the values of  $C_L$  were not symmetrical with  $90^\circ$  seems to be the influence of the tower. The clear difference in the values of  $C_D$  and  $C_L$  by surface roughness wasn't observed. The differences caused by wind velocity on  $C_D$  and  $C_L$  are shown in Figure 8(a) and (b). Even if the wind velocity was

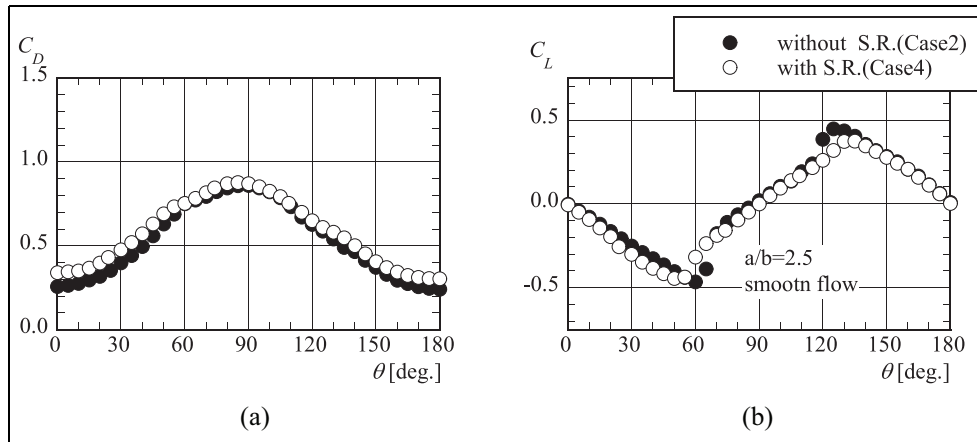


**Figure 7.** Effects of surface roughness on (a)  $C_D$  and (b)  $C_L$  in a smooth flow: S.R. in the legend means surface roughness.

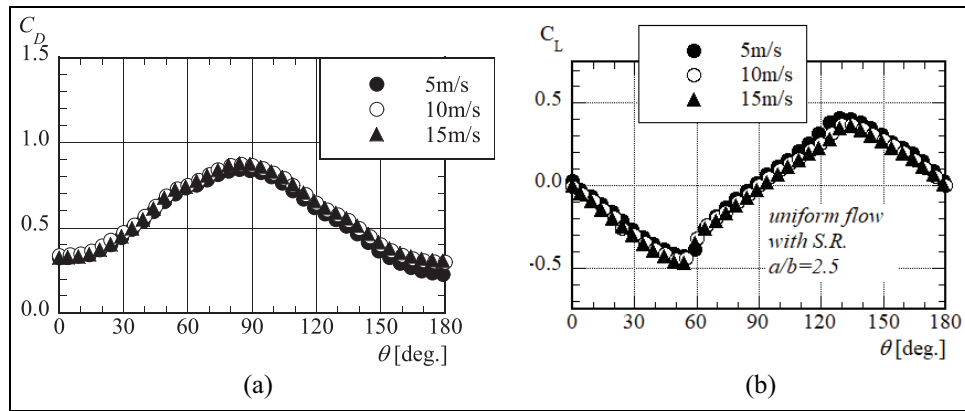


**Figure 8.** Effects of wind velocity on (a)  $C_D$  and (b)  $C_L$  in a smooth flow.

changed as 5, 10, and 15 m/s, differences on  $C_D$  and  $C_L$  were very slight and no drastic change could be seen. The effects of Reynolds number, therefore, were very slight in the range of this experiment.

The effects of inflow turbulence in case of aspect ratio  $a/b = 2.5$  (Case4 and Case8) are shown in Figure 9(a) and (b). Affection by inflow turbulence on  $C_D$  and  $C_L$  were also very slight. The values of  $C_L$  are almost same between smooth flow and turbulence boundary flow. As for  $C_D$ , the values in turbulence boundary flow were smaller slightly than that in smooth flow. This reduction of  $C_D$  in turbulence boundary flow is typical phenomena for bluff body, such as rectangular cylinder (Noda and Nakayama, 2003). The reason is that the wake decreases and the pressure on the surface behind recover caused by turbulence in the incident flow.

Figure 10(a) and (b) show the effects of nacelle lengths on  $C_D$  and  $C_L$ . By means of defining  $C_D$  and  $C_L$  using equation (3) which is projection area at the angle  $90^\circ$ , the influence of nacelle length on  $C_D$  and  $C_L$  becomes quite small, with or without surface roughness. It seems that characteristics of  $C_D$  and  $C_L$  are mostly independent of the aspect ratios.

### Formulas for mean wind force coefficients

Formulas for the mean drag and lift force coefficients of nacelles can be expressed as a function of yaw angle only, since the characteristics of  $C_D$  and  $C_L$  are nearly independent of the aspect ratios. The wind force coefficients for an extreme wind load that acts on the nacelles are expressed as in equations (4) and (5).

$$C_D(\theta) = -0.21 \cos(2.1\theta) + 0.67 \quad (4)$$

$$C_L(\theta) = \{-0.5 \sin(2\theta) + 0.06 \sin(0.5\theta)\} \cdot \{1.2 + 0.1 \cos(4\theta)\} \cdot \cos(0.35\theta) \quad (5)$$

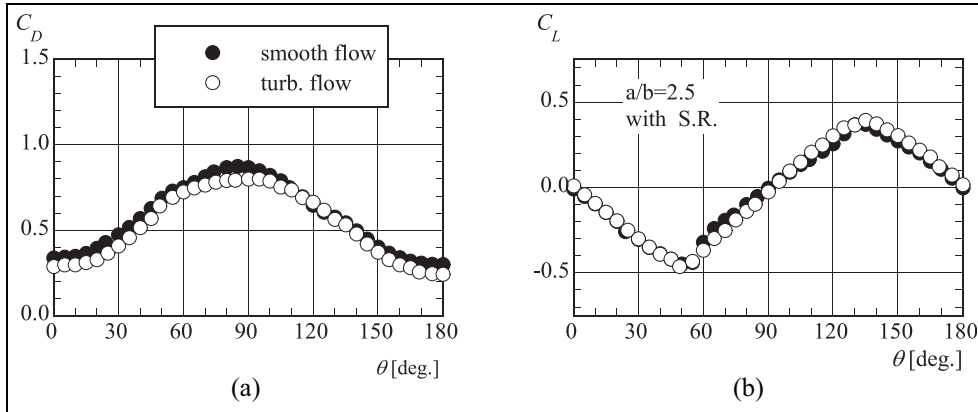


Figure 9. Effects of turbulence in incident flow on (a)  $C_D$  and (b)  $C_L$ : S.R. means surface roughness.

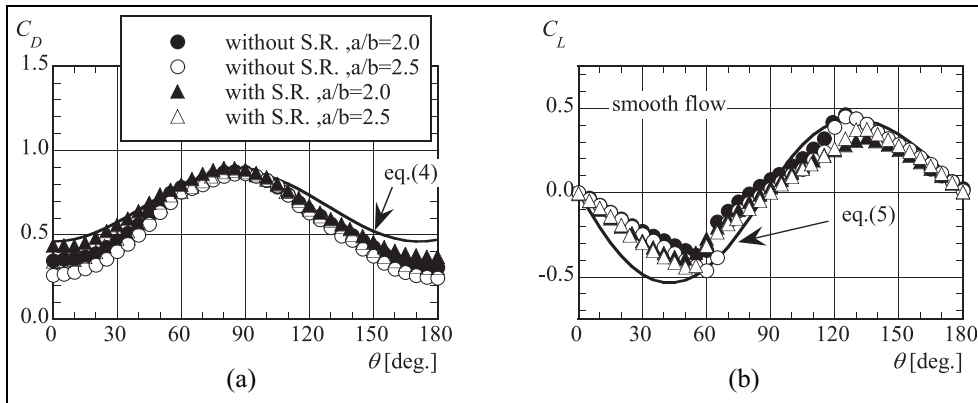


Figure 10. Effects of nacelle lengths on (a)  $C_D$  and (b)  $C_L$  in a smooth flow: S.R. in the legend means surface roughness.

The comparison between the proposed formulas for wind force coefficients and experimental results in the range of yaw angle  $\theta = 0^\circ$  to  $\theta = 180^\circ$  are shown in Figure 10. Equations (4) and (5) are in good agreement with the experimental results. To simplify the formulas, these proposed formulas are represented with trigonometric functions. Therefore, some deviations from the experimental results are observed. The proposed formulas provide slightly conservative results, in particular  $C_L$  become large value around  $45^\circ$ .

The value of  $C_D$  recommended by Germanischer Lloyd (2010) is 1.3 (in supposing the shape as rectangle, because no other suitable shape) and that of Eurocode (2005) is 0.6 (in supposing the shape as sphere and Reynolds number as  $10^5$ ). From Figure 10, it can be seen that the maximum value of  $C_D$  obtained by wind tunnel experiment is 0.9. The reference area used in Germanischer Lloyd (2010) is project area as a function of the yaw angle. For comparison,  $C_D$  at the angle  $0^\circ$  is recalculated using project area at the angle  $0^\circ$  and the values of  $C_D$  in Figure 10 become about 0.9. This indicates that  $C_D$  of 1.3 recommended by Germanischer Lloyd (2010) is overestimated for ellipsoidal nacelles. As for Eurocode (2005), recommended value 0.6 for  $C_D$  seems to be underestimated. As for ASCE7-16 (2016), it might be possible to refer the mean drag coefficients for solid freestanding walls, solid freestanding signs, chimneys, tanks, and similar structures. The values are 1.8 in case of aspect ratio  $B/s = 2$  and clearance ratio  $s/h < 0.16$ , and 0.6 in case of round, moderately smooth, aspect ratio  $h/D = 7$ , respectively. However, these values also overestimate or underestimate the mean drag coefficients from the wind tunnel tests depending on the wind direction.

### Pressure coefficients

Characteristics of the peak pressure coefficients are investigated based on surface pressure measurements. There are two design load cases for extreme wind in IEC (IEC 61400-1, 2019) those are DLC 6.1 and DLC 6.2. DLC 6.1



is the design load case for a wind turbine with an active yaw system in which a yaw misalignment of up to  $\pm 15^\circ$  should be considered. DLC 6.2 assumes the loss of electrical power for control of the yaw system. In this situation, the effects of the yaw angle changing up to  $\pm 180^\circ$  should be considered. Peak pressure coefficients for these two design load cases are discussed in this section. Distributions of the equivalent maximum and minimum mean pressure coefficients for the design of the nacelle covers are proposed and compared with the mean pressure coefficients provided by Germanischer Lloyd (2010).

### Definitions of pressure coefficients

The mean pressure coefficient at yaw angle  $\theta_i$ , of each point  $j$  is defined as below.

$$\bar{C}_{p_j}(\theta_i) = \frac{\bar{p}_j(\theta_i) - p_{ref}}{\frac{1}{2}\rho U_h^2} \quad (6)$$

where  $\bar{C}_{p_j}(\theta_i)$  is mean pressure coefficient at point  $j$  and yaw angle  $\theta_i$ ,  $\bar{p}_j(\theta_i)$  is mean (i.e. time averaged) pressure at point  $j$  and yaw angle  $\theta_i$ .  $\theta_i$  is the yaw angle,  $U_h$  is the wind velocity at the nacelle height and  $p_{ref}$  is the reference pressure. The reference pressure was measured by a pitot tube placed 1.3 m upstream from the nacelle model.

The maximum and minimum peak pressure coefficients at yaw angle  $\theta_i$ , of each point  $j$  are defined as below, respectively.

$$\hat{C}_{p_{max,j}}(\theta_i) = \frac{\hat{p}_{max,j}(\theta_i) - p_{ref}}{\frac{1}{2}\rho U_h^2} \quad (7)$$

$$\hat{C}_{p_{min,j}}(\theta_i) = \frac{\hat{p}_{min,j}(\theta_i) - p_{ref}}{\frac{1}{2}\rho U_h^2} \quad (8)$$

where,  $\hat{C}_{p_{max,j}}(\theta_i)$  and  $\hat{C}_{p_{min,j}}(\theta_i)$  are maximum and minimum peak pressure coefficients at point  $j$  and yaw angle  $\theta_i$ , respectively.  $\hat{p}_{max,j}(\theta_i)$  and  $\hat{p}_{min,j}(\theta_i)$  are maximum and minimum peak pressures at point  $j$  and yaw angle  $\theta_i$ , respectively.

The maximum ( $\hat{C}_{p_{max,j}}$ ) and minimum ( $\hat{C}_{p_{min,j}}$ ) peak pressure coefficients during the entire yaw angles are defined as in equations (9) and (10), respectively. These coefficients correspond to DLC 6.2 in IEC61400-1.

$$\hat{C}_{p_{max,j}} = \text{Max}\{\hat{C}_{p_{max,j}}(\theta_1), \dots, \hat{C}_{p_{max,j}}(\theta_i), \dots, \hat{C}_{p_{max,j}}(\theta_n)\} \quad (9)$$

$$\hat{C}_{p_{min,j}} = \text{Min}\{\hat{C}_{p_{min,j}}(\theta_1), \dots, \hat{C}_{p_{min,j}}(\theta_i), \dots, \hat{C}_{p_{min,j}}(\theta_n)\} \quad (10)$$

The maximum ( $\hat{C}_{p_{max,j}}(\pm 15^\circ)$ ) and minimum ( $\hat{C}_{p_{min,j}}(\pm 15^\circ)$ ) peak pressure coefficients for yaw angles ranging from  $-15^\circ$  to  $+15^\circ$  are defined as in equations (11) and (12). These coefficients correspond DLC 6.1 in IEC61400-1.

$$\hat{C}_{p_{max,j}}(\pm 15^\circ) = \text{Max}\{\hat{C}_{p_{max,j}}(-15^\circ), \dots, \hat{C}_{p_{max,j}}(15^\circ)\} \quad (11)$$

$$\hat{C}_{p_{min,j}}(\pm 15^\circ) = \text{Max}\{\hat{C}_{p_{min,j}}(-15^\circ), \dots, \hat{C}_{p_{min,j}}(15^\circ)\} \quad (12)$$

### Mean and peak pressure coefficients

The contours of mean, maximum peak, and minimum peak pressure coefficients at typical yaw angles, that is,  $0^\circ$ ,  $60^\circ$ , and  $300^\circ$ , in side view of nacelle are shown in Figures 11 to 13, respectively. The maximum values of the mean pressure coefficient on the surface of nacelle are approximately 0.8 which occur around the stagnation point, that is, the left edge in case of (a) yaw angle of  $0^\circ$ , the left side on the middle height in case of (c) yaw angle of  $300^\circ$ , no stagnation point in case of (b) yaw angle of  $60^\circ$  because it is on downwind side. As the distance from that point increases, the mean pressure coefficient decreases. They are beyond 0 and become negative value. The distributions of the maximum peak pressure coefficients are generally similar to that of the mean pressure coefficients in all yaw angle. However, the values themselves are different from the mean pressure coefficients, and the maximum values of the maximum peak pressure coefficients at each yaw angle are slightly less than 1.8.

The distributions of the minimum peak wind pressure coefficient have tendency similar to that of the mean pressure coefficient. However, they are not as similar as those of the maximum peak pressure coefficient. Regarding

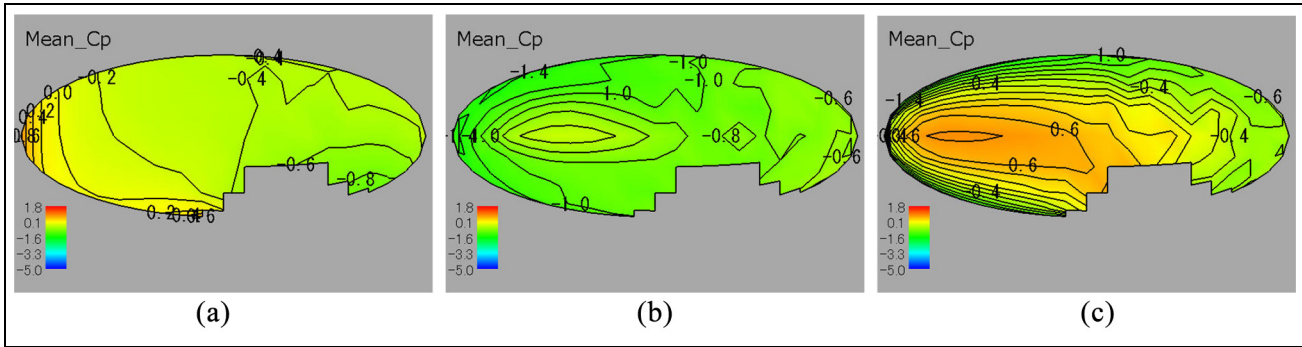


**Figure 11.** Distributions of mean pressure coefficients in side view: (a) at yaw angle of 0°, (b) at yaw angle of 60°, and (c) at yaw angle of 300°.

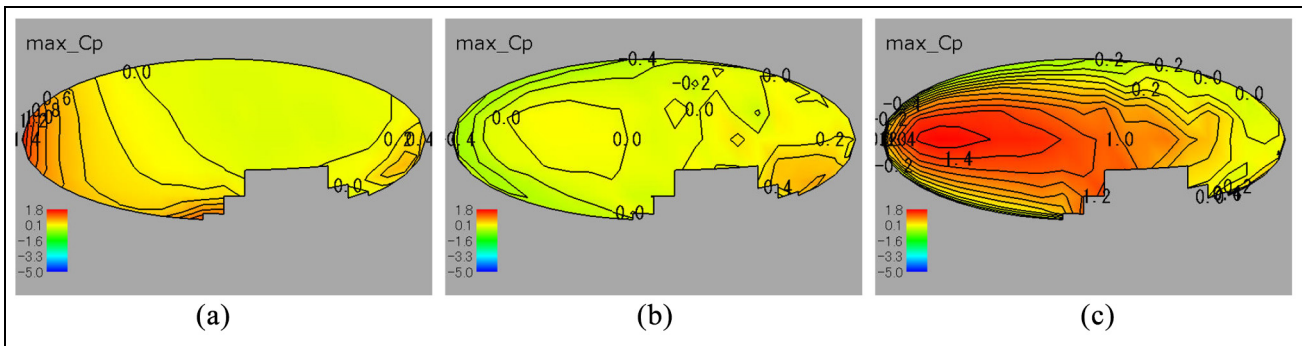


**Figure 12.** Distributions of maximum peak pressure coefficients in side view: (a) at yaw angle of 0°, (b) at yaw angle of 60°, and (c) at yaw angle of 300°.

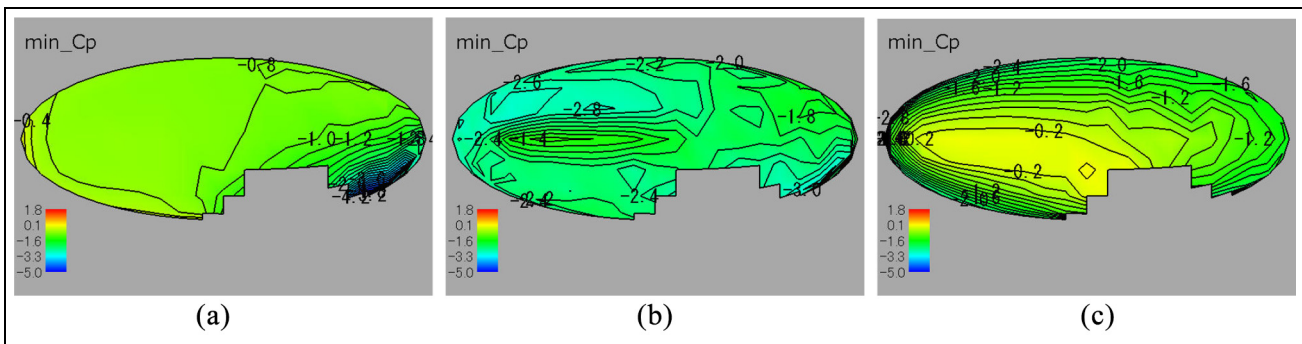


**Figure 13.** Distributions of minimum peak pressure coefficients in side view: (a) at yaw angle of 0°, (b) at yaw angle of 60°, and (c) at yaw angle of 300°.

the minimum peak pressure coefficient, strong negative peak pressure coefficients are occurred on the downwind side near the tower due to the influence of the tower. For instance, strong negative peak pressure coefficients can be seen in the lower right area of the nacelle at yaw angle of 0° in Figure 13(a). Figures 11 to 13 show about the only typical yaw angles, but the tendencies described above can be also said concerning all yaw angle cases.

The contours of maximum and minimum peak pressure coefficients at all yaw angles are shown in Figures 14 and 15, respectively. The values of maximum peak pressure coefficients on front, side, and rear surface are slightly over 1.8 at the height of nacelle center, and decrease toward top and bottom. These characteristics also can be

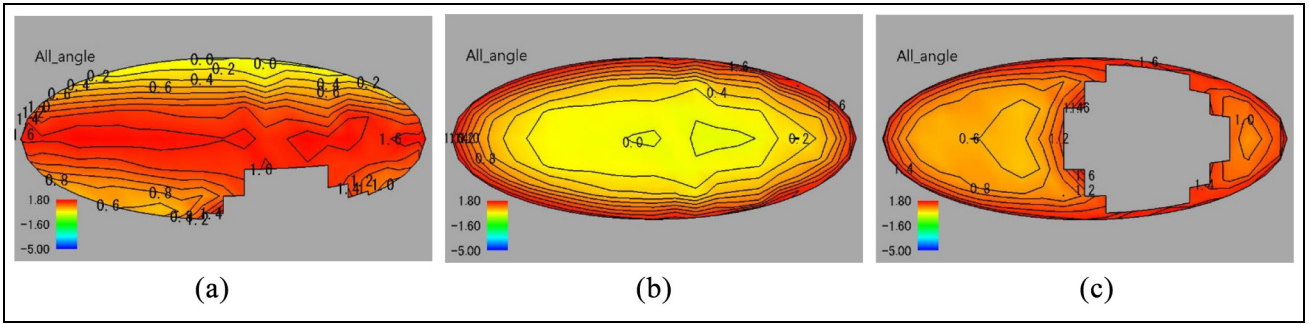


Figure 14. Maximum peak pressure coefficients for the entire range of yaw angle: (a) side view, (b) top view, and (c) bottom view.

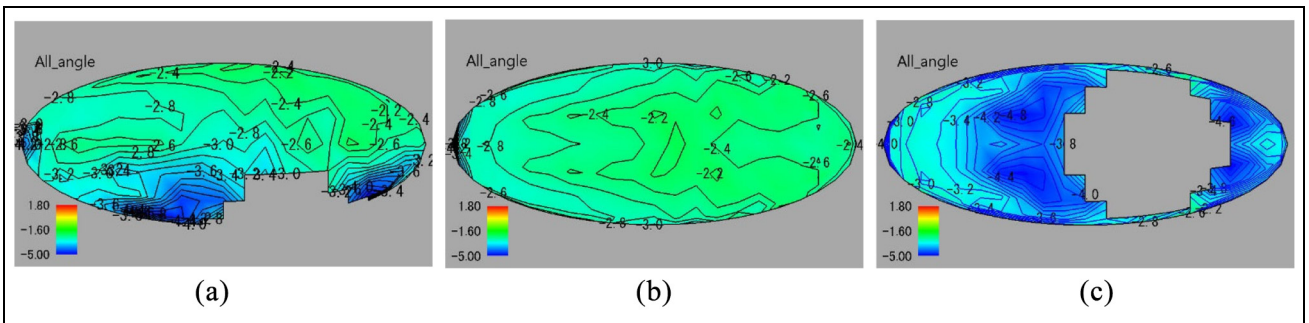


Figure 15. Minimum peak pressure coefficients for the entire range of yaw angle: (a) side view, (b) top view, and (c) bottom view.

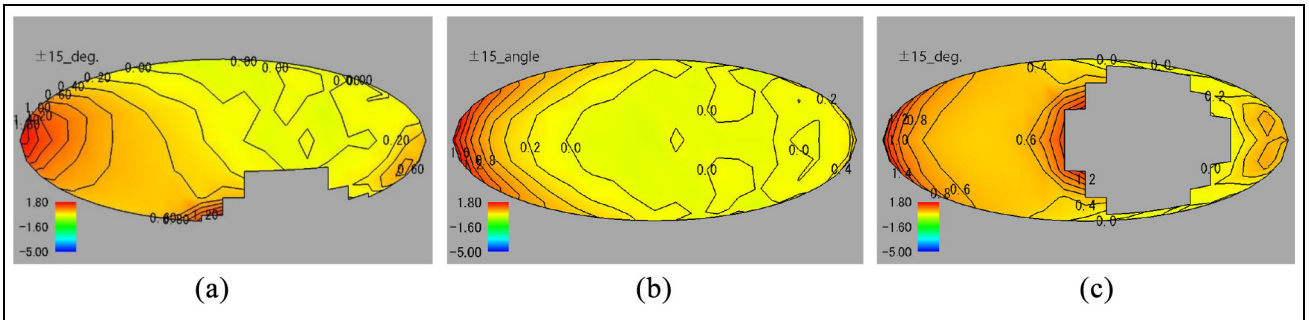
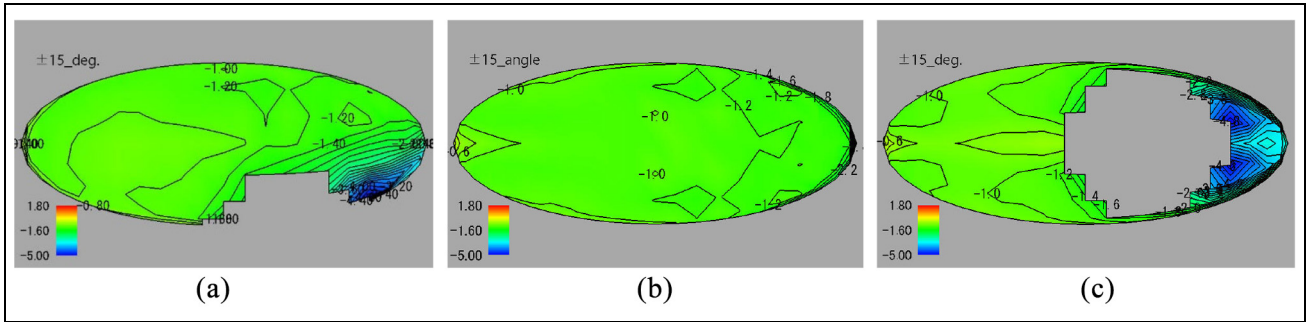


Figure 16. Maximum pressure coefficient for yaw angle range from  $-15^\circ$  to  $+15^\circ$ : (a) side view, (b) top view, and (c) bottom view.

found in case of rectangular type nacelles investigated by Noda and Ishihara (2014). On the top surface of nacelle, the maximum value was almost 0.0 and never become a negative value. On the lower area, the values of maximum peak pressure coefficients are larger than those on the top surface due to the influence of the tower.

As for minimum peak pressure coefficients, the distributions were more complex than maximum peak pressure coefficients. The large local peak pressure coefficients were observed at the front edge of the nacelle, with the value of  $-4.4$ . The large negative peak pressure coefficients were also observed on the lower area near the tower and the values range from  $-4.4$  to  $-4.8$ . On the side surface of nacelle, the distribution of minimum peak pressure coefficients were almost uniform, the values on side surfaces were slightly larger than those on the top surface of the nacelle.

The maximum and minimum peak pressure coefficients for yaw angles ranging from  $-15^\circ$  to  $+15^\circ$  are shown in Figures 16 and 17, respectively. In case of restricted the yaw angles, large values of maximum peak pressure coefficients are limited in the front region of nacelle. As for the minimum peak pressure coefficients, local peak suction influenced by the tower appeared only downwind of the tower.



**Figure 17.** Minimum pressure coefficient for yaw angle range from  $-15^\circ$  to  $+15^\circ$ : (a) side view, (b) top view, and (c) bottom view.

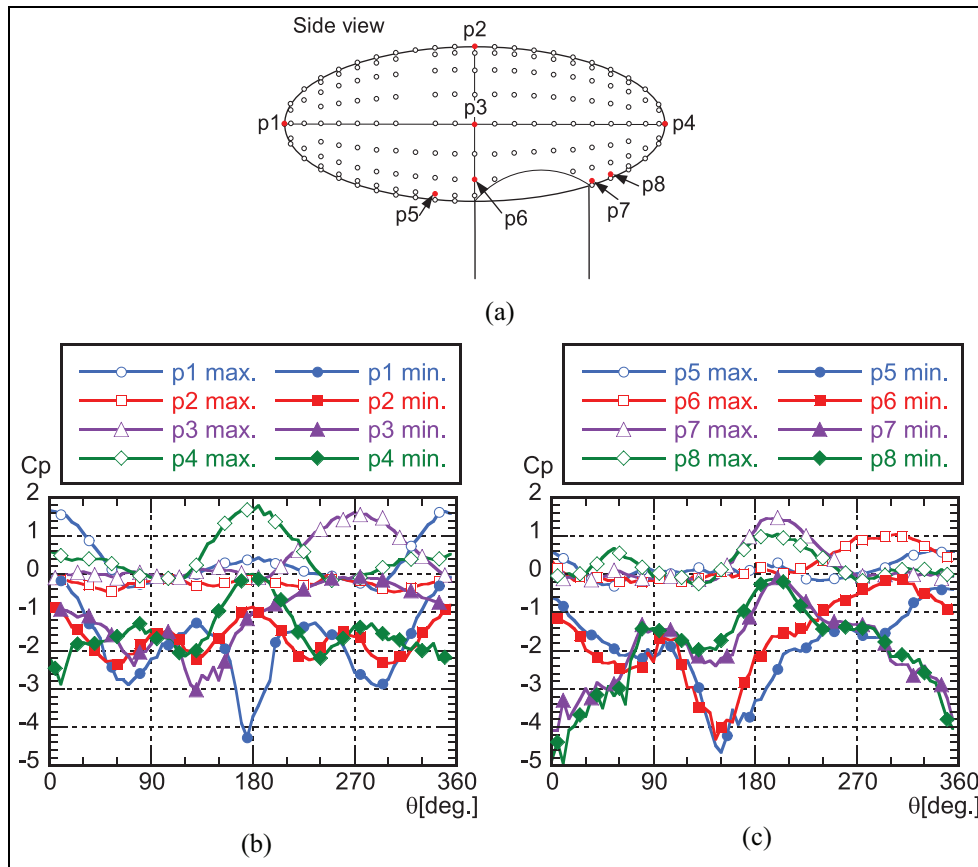


**Figure 18.** Variations of maximum and minimum peak pressure coefficients: (a) locations where the wind pressure coefficients are plotted, (b) typical points, and (c) points around the tower.

The maximum and minimum peak pressure coefficients versus the yaw angle at typical points “p1–p4” and points around the tower “p5–p8” are shown in Figure 18. Large negative peak pressure at “p1” in the vicinity of front edge are observed at yaw angle around  $180^\circ$ , the point “p1” was behind tower at this yaw angles. Mean pressure coefficient at “p1”, were not so large negative values around  $180^\circ$ . At the point “p3” on middle of side and at “p4” on middle of rear of nacelle, no extreme negative peak pressures appeared, even if these points were at yaw angle downwind of the tower. At the point “p2” on the top of nacelle, extreme negative and positive peak pressures were not observed. On the top of nacelle, the positive values in the maximum peak pressure coefficients almost can’t be seen. On the side of nacelle at the point of “p3,” no extreme peak pressures appeared. At the point of “p3,” positive peak pressure coefficients became maximum values around the angle in which surface of

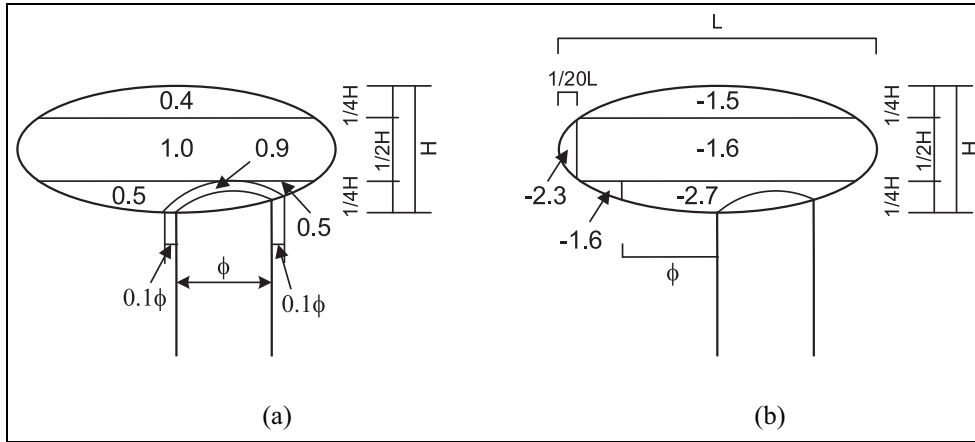


**Figure 19.** Equivalent maximum (a) and minimum (b) mean pressure coefficients proposed for DLC 6.2.

measurement points were normal to the wind direction and negative peak pressure coefficients took minimum values at the angle slightly deviated from parallel wind direction. On the bottom area near the tower at the points of “p5–p8,” extreme negative peak pressure can be found. These strong negative pressure peaks occurred at the angle in which each measurement point reached to the leeward side of the tower, and strongest values were appeared at the region slightly away from the tower, such as p5 and p8. It can be found that surface pressure around the tower are significantly influenced by the tower.

**Formulas for equivalent mean pressure coefficients and comparison with current codes**

Since the maximum peak pressures are primarily dominated by the incident turbulence, a quasi-steady assumption (Holmes, 2007) is applicable to estimate the maximum peak pressure coefficients. In fact, distributions of the maximum peak pressure coefficients on all of the surfaces are similar to those of the maximum mean pressure coefficients. It is difficult to apply a quasi-steady assumption to the minimum peak pressure coefficients, since the minimum peak pressure coefficients are caused by not only incident turbulence but also vortex shedding. To avoid complications in determination of wind load, the quasi-steady assumption is adopted as in Eurocode (2005) and both of the equivalent maximum and minimum mean pressure coefficients are determined in consideration of the turbulence intensity of the incident flow. Owing to the using the equivalent maximum and minimum mean pressure coefficients, it is possible to evaluate positive and negative peak pressure coefficients according to various turbulence intensities.

The equivalent maximum ( $\bar{C}pe_{max}$ ) and minimum ( $\bar{C}pe_{min}$ ) mean pressure coefficients are defined as in equations (13) and (14), respectively.

$$\bar{C}pe_{max} = \frac{\hat{C}p_{max}}{1 + 7I_h} \tag{13}$$

$$\bar{C}pe_{min} = \frac{\hat{C}p_{min}}{1 + 7I_h} \tag{14}$$

$I_h$  is the turbulence intensity at the nacelle height, expressed as follows:

$$I_h = \frac{\sigma_1}{U_h} \tag{15}$$

where  $\sigma_1$  is the standard deviation of the along wind component of the incident flow. The equivalent maximum and minimum mean pressure coefficients are proposed in Figure 19 for DLC 6.2 in IEC61400-1 (2019). These values are calculated using equations (13) and (14), the turbulence intensity (13%) of incident flow at the nacelle height and the maximum and minimum peak pressure coefficients shown in Figures 14 and 15.



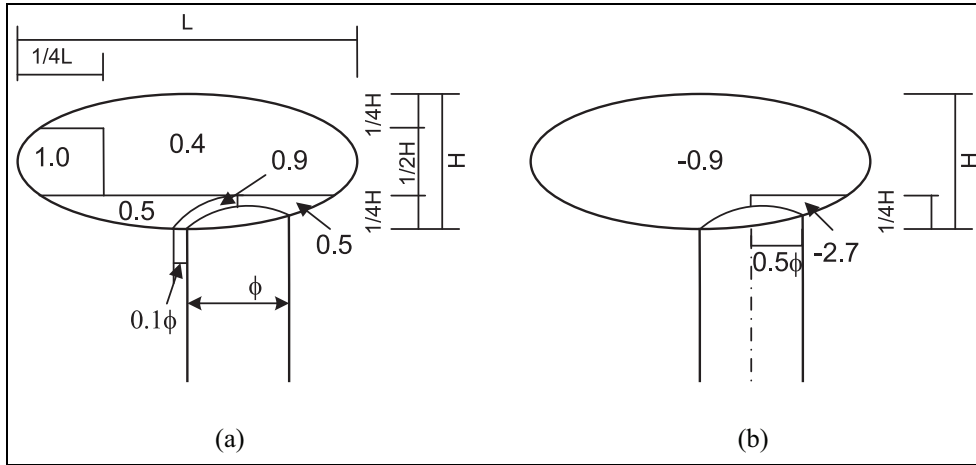


**Figure 20.** Equivalent maximum (a) and minimum (b) mean pressure coefficients proposed for DLC 6.1.

The equivalent maximum  $\bar{C}_{pe_{\max}(\pm 15^\circ)}$  and minimum  $\bar{C}_{pe_{\min}(\pm 15^\circ)}$  mean pressure coefficients for yaw angles ranging from  $-15^\circ$  to  $+15^\circ$  are also defined as in equations (16) and (17), respectively.

$$\bar{C}_{pe_{\max}(\pm 15^\circ)} = \frac{\hat{C}_{p_{\max}(\pm 15^\circ)}}{1 + 7I_h} \quad (16)$$

$$\bar{C}_{pe_{\min}(\pm 15^\circ)} = \frac{\hat{C}_{p_{\min}(\pm 15^\circ)}}{1 + 7I_h} \quad (17)$$

Figure 20 shows the proposed equivalent mean pressure coefficients corresponding to the DLC 6.1 in IEC61400-1 (2019). Figure 20 is also based on equations (16), (17), and the wind tunnel test results shown in Figures 16 and 17. The turbulence intensity of incident flow at the nacelle height were also used.

In the case of yaw angles ranging from  $-15^\circ$  to  $+15^\circ$ , the region taking large values become small as for both maximum and minimum equivalent mean pressure coefficient. Regarding equivalent maximum mean pressure coefficients, the largest value of 1.0 is limited to the front area of the nacelle, and the smallest value of  $-2.7$  of equivalent minimum mean pressure coefficients is limited to the area behind of the tower.

The mean pressure coefficients proposed in Germanischer Lloyd (2010) are considerably small for maximum and minimum mean pressure coefficients compared with those from the wind tunnel tests. The distribution of mean pressure coefficients recommended by Germanischer Lloyd (2010) are not in consideration of local peak pressures. Furthermore, since the mean pressure coefficients recommended by Germanischer Lloyd (2010) assumes a rectangular type nacelle, it is difficult to apply to an ellipsoidal nacelle.

## Conclusion

Wind tunnel experiments are performed for measurements of the mean wind forces acting on ellipsoidal nacelles for wind resistant design of wind turbines. The peak pressures acting on an ellipsoidal nacelle are also measured to investigate the equivalent maximum and minimum mean pressure coefficients for design of cover and hatch on the ellipsoidal nacelle. The results are compared with current codes such as Eurocode (2005), Germanischer Lloyd (2010), and ASCE7-16 (2016). The following conclusions are obtained from this study.

The effects of Reynolds number on wind force coefficients  $C_D$  and  $C_L$  are not observed clearly and the effects of the turbulence in the incident flow and nacelle length are negligible. Formulas for  $C_D$  and  $C_L$  as functions of yaw angles are proposed. The mean wind force coefficients of 1.3 in Germanischer Lloyd (2010) seems to be overestimated and 0.6 in Eurocode (2005) is underestimated, comparing with those obtained from the wind tunnel experiments. ASCE7-16 (2016) also overestimates or underestimates the wind force coefficients depending on the wind direction.

The equivalent maximum and minimum mean pressure coefficients are proposed for DLC6.1 and DLC6.2 in IEC61400-1 (2019) based on the pressure measurements. The equivalent maximum and minimum mean pressure coefficients are proposed based on the quasi-steady theory to take the turbulence intensity into account. The proposed equivalent maximum and minimum mean pressure coefficients are much larger than those proposed in Germanischer Lloyd (2010).


### Declaration of conflicting interests

The author(s) declared no potential conflicts of interest with respect to the research, authorship, and/or publication of this article.

### Funding

The author(s) received no financial support for the research, authorship, and/or publication of this article.

### ORCID iD

Hiroshi Noda  <https://orcid.org/0000-0001-8751-9646>

### References

- Abbott IH and Von Doenhoff AE (1959) *Theory of Wind Section Including a Summary of Airfoil Data*. New York, NY: Dover Publications, Inc.
- ASCE/AWEA RP (2011) Recommended practice for compliance of large land-based wind turbine support structures. *American Wind Energy Association and American Society of Civil Engineers*.
- ASCE7-16 (2016) *Minimum Design Loads for Buildings and Other Structure*. Standard American Society of Civil Engineers.
- Buresti G (1981) The effect of surface roughness on the flow regime around circular cylinders. *Journal of Wind Engineering and Industrial Aerodynamics* 8: 105–114.
- Chou JS, Chiu CK, Huang IK, et al. (2013) Failure analysis of wind turbine blade under critical wind loads. *Engineering Failure Analysis* 27: 99–118.
- Esfahanian V, Salavati Pour A, Harsini I, et al. (2013) Numerical analysis of flow field around NREL phase II wind turbine by a hybrid CFD/BEM method. *Journal of Wind Engineering and Industrial Aerodynamics* 120: 29–36.
- Eurocode (2005) Actions on structures, part 1-4. General actions—Wind actions. European Committee for Standardization.
- Germanischer Lloyd (2010) Guideline for the certification of wind turbines. *Germanischer Lloyd Industrial Services GmbH, Renewables Certification*. Brooktorkai 18, 20457 Hamburg, Germany.
- Goit JP and Ishihara T (2020) Aerodynamic loads on wind turbine nacelles under different inflow turbulence conditions. *Wind Energy* 23: 645–659.
- Holmes JD (2007) *Wind Loading of Structures*. London and New York, NY: Taylor & Francis.
- Hu H, Yang Z and Sarkar P (2012) Dynamic wind loads and wake characteristics of a wind turbine model in an atmospheric boundary layer wind. *Experiments in Fluids* 52: 1277–1294.
- IEC 61400-1 (2019) *Wind Energy Generation Systems – Part 1: Design Requirement*. International Electrotechnical Commission. Genève.
- Irwin HP, Cooper KR and Girard R (1979) Correction of distortion effects caused by tubing systems in measurements of fluctuating pressures. *Journal of Wind Engineering and Industrial Aerodynamics* 5: 93–107.
- Ishihara T (ed.) (2010) *Guidelines for Design of Wind Turbine Support Structures and Foundations*. Tokyo, Japan: Japan Society of Civil Engineers, (in Japanese).
- Ishihara T, Yamaguchi A, Takahara K, et al. (2005) An analysis of damaged wind turbines by typhoon Maemi in 2003. In: *Proceedings of APCWE VI*, Seoul, Korea, 12–14 September, pp.1413–1428.
- Lawson TV (1980) *Wind Effects on Buildings Volume 1 Design Applications*. London: Applied Science Publisher LTD.
- Lee JW, Lee JS, Han JH, et al. (2012) Aero-elastic analysis of wind turbine blades based on modified strip theory. *Journal of Wind Engineering and Industrial Aerodynamics* 110: 62–69.
- METI of Japan (2016) Wajima wind farm number 2 wind turbine nacelle cover damage report. Available at: [https://www.meti.go.jp/shingikai/sankoshin/hoan\\_shohi/denryoku\\_anken/newenergy\\_hatsuden\\_wg/pdf/010\\_02\\_00.pdf](https://www.meti.go.jp/shingikai/sankoshin/hoan_shohi/denryoku_anken/newenergy_hatsuden_wg/pdf/010_02_00.pdf) (accessed 10 August 2021, in Japanese).
- METI of Japan (2017) Minamiosumi wind farm nacelle cover damage report. Available at: [https://www.meti.go.jp/shingikai/sankoshin/hoan\\_shohi/denryoku\\_anken/newenergy\\_hatsuden\\_wg/pdf/012\\_04\\_00.pdf](https://www.meti.go.jp/shingikai/sankoshin/hoan_shohi/denryoku_anken/newenergy_hatsuden_wg/pdf/012_04_00.pdf) (accessed 10 August 2021, in Japanese).
- Noda H and Ishihara T (2014) Wind tunnel test on mean wind forces and peak pressures acting on wind turbine nacelles. *Wind Energy* 17: 1–17.

- Noda H and Nakayama A (2003) Free-stream turbulence effects on the instantaneous pressure and forces on cylinders of rectangular cross section. *Experiments in Fluids* 34: 332–344.
- Ohkuma T, Marukawa H and Miyashita K (1986) An experimental study on turbulent boundary layer developed over the urban area. In: *Proceedings of the 9th national symposium on wind engineering*, Tokyo, Japan, 4–6 December, pp.61–66 (in Japanese).
- Rafiee R, Tahani M and Moradi M (2016) Simulation of aeroelastic behavior in a composite wind turbine blade. *Journal of Wind Engineering and Industrial Aerodynamics* 151: 60–69.
- Rajani BN, Kandasamy A and Majumdar S (2016) LES of flow past circular cylinder at  $Re = 3900$ . *Journal of Applied Fluid Mechanics* 9(3): 1421–1435.
- Roshko A (1961) Experiments on the flow past a circular cylinder at very high Reynolds number. *Journal of Fluid Mechanics* 10(3): 345–356.
- Schmitz FW (1942) Aerodynamics of the model airplane. Part I airfoil measurements. Translated at Redstone Scientific Information Center RSIC-721 (1967).
- Williamson CHK (1996) Vortex dynamics in the cylinder wake. *Annual Review of Fluid Mechanics* 28: 477–539.